Investigation on magneto-thermal-structural coupled field effect of nano coated 230 kV busbar

S Victoria Mary and C Pugazhendhi Sugumaran

Division of High Voltage, Anna University, Chennai, India

E-mail: victoriamary@annauniv.edu.in

Abstract

The coupled field, Magnetic-thermal-structural analysis has been carried out for 230 kV bare and nano Fe coated busbar. The integrated coupled field analytical equations were developed by using electrical parameters to predetermine the temperature rise and mechanical stress. The finite element method software ANSYS APDL commercial package has been used for simulation analysis with magneto-thermal-structural sequential weak coupling methods. The 6061-T6 hollow aluminium busbar size of 1 m length and 8 mm thickness with the load current of 1000 A was modelled and the magnetic field effect was analysed through magnetostatic solver. From the analysis, it was inferred that the nano iron coated busbar diminishes the magnetic field around 80% in the vicinity areas. The magnetic field reduction is achieved by high conductivity and high permeability of the material. It also reduces the rise of temperature by 4 °C with the property of high thermal conductivity, thus reduces the thermal flux by 50 W m^{-2}. Thermal dependent mechanical stress is decreased by 35% for coated conductor compare with the bare conductor. Due to the thermal expansion coefficient, the coated material aid to protect the busbar against the mechanical stress. The simulation results were analyzed and compared with the analytical results. The nano coated conductor exhibit the low electromagnetic pollution in the environment by reducing the electromagnetic field and temperature rise.

Supplementary material for this article is available online

Keywords: busbars, coupled field, sequential finite element method, substations, nano Fe coating

(Some figures may appear in colour only in the online journal)

1. Introduction

Nowadays electric field (EF) and magnetic field (MF) pollution are constantly increasing in the vicinity areas around substation and Transmission lines [1]. Manmade EF and MF are mutely growing in the world. Humans are continuously exposed to the electromagnetic environment from the domestic appliance and industrial equipment [2]. The EF and MF exposure to the human body results in energy absorption and internal body currents [3]. According to World Health Organization (WHO), the electromagnetic field from power system causes short term and long term health problems. So the studies of electromagnetic field impact in the living system are required.

Due to populace growth, the high voltage substation keeps increasing in the rural area. The modernization in the power system, escalate the highly complex and intricate network [1, 4]. The primary and secondary equipment in the substation is act as the source and victim of the electromagnetic environment [3–5]. It causes a higher amount of emission through MF, EF, and heat flux (HF) which seriously affect the substation equipment and living things (human, plants and animals) in the ecosystem. Currently, researchers focused on the extra high voltage (EHV)/ultra high voltage (UHV) substation electromagnetic smog [6–10]. The standards are provided by many international organization and several countries [5, 8–11]. There is no universal standard for substation electromagnetic environment. The ICNIRP has set

1

the public and occupation exposure limit for EF, MF and HF to human being [3].

In a substation, the busbar plays a vital role in transporting the current and voltage from incoming feeder to outgoing feeder. The busbar is the primary candidate to distribute the energy and supply in and around the substation. The busbar makes the electrical energy distribution more flexible and less expensive [12]. It is mostly used in high voltage applications. The busbar should be withstood against transient conditions and temperature rise for high voltage and high current without having a mechanical failure.

The temperature has to be considered as a crucial factor in deciding the busbar diameter, surface area and current carrying capacity. These are the essential parameter to design the busbar. The degree of mechanical flexibility must be higher to withstand the short circuit conditions. In short circuit conditions, the magnetic force and temperature will rise sharply [13, 14]. The hollow busbars are commonly used to dissipate more heat through the large cross-sectional area. More literature shows the detailed analysis for the rectangular and gas insulated substation (GIS) busbars [12–15].

In this article, the extremely low frequency (ELF) magnetic field reduction technique was proposed [16]. The high frequency electromagnetic field (EMF) reduction techniques are available commercially [17–20]. But power frequency (50/60 Hz) MF shielding is still in research [20–25]. This paper proposed the power frequency magnetic field mitigation technique by using ferromagnetic material. The nano iron is used to mitigate the magnetic field. The magnetic shielding is achieved by nano coating on the busbar. The shielding material is described in chapter 2.

In this modelling, integrated coupled field equation was developed. The coupled field analysis will enhance the integrity of real-time scenario [26–32]. The multiphysics analysis can eliminate the real-world product failure. In this work, we used magneto-thermal-structural (M-T-S) [26–28, 32] and magneto-structural (M-S) analysis. In ANSYS, sequential finite element method (FEM) is executed as unidirectional flow.

The magnetic field intensity (H), magnetic flux density (B), magnetic force (MF), temperature rise (T), Thermal gradient (TG), Thermal flux (HF), Stress and Strain have been determined by using analytical formula and simulation. The values of magnetic field effect are given as input for thermal analysis. Further, the thermal results are given as input for the structural analysis [13–15, 30, 31]. It is illustrated in chapter 3. The sequential FEM results were compared with analytical values.

2. Application of soft magnetic alloys for field reduction

Soft magnetic materials are generally used for magnetic shielding. It is easily magnetized and demagnetized. The temperature rise and current capacity will decide the shape and size of the
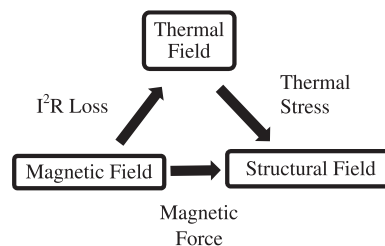

Figure 1. Coupled field sequential FEM analysis of busbar.

busbar [11–13, 32]. The insulation coating for busbar will reduce the current carrying capacity of the busbar [14]. So the high permeability and high conductivity material is used for shielding to reduce the magnetic field [17–20]. Commercially available soft magnetic alloys are NANOPERM, NANOPERN, VITROVAC, FINEMET, VITROPERM, PERMALLOY and MUMETAL [19]. These are the combination of Fe–Cu–Nb–B–P–Si–Mo–Ni alloy in different proportion. Those are used for high frequency magnetic shielding. But for low frequency tin–lead, copper alloy, super conductivity material [23] and silver coatings are used.

In this study, nano Fe coating is used as power frequency (50 Hz) magnetic shielding. Because ferromagnetic alloys having high permeability and low coercivity compare with other alloys [18–20]. The nano crystalline iron based alloys have higher saturation magnetization. It is less expensive and abundantly available on the earth. Iron based metallic alloys increase the magnetic properties and thermal properties. It has the unique property of superparamagnetic in nature. It will occur only in small grain size iron based metals. The iron based alloys enhance the thermal properties and structural properties. NANOPERM soft magnetic alloy also has the magnetic shielding properties at power frequency [20].

3. Integrated coupled-field formulation

Coupled-Field generally used in multiphysics problems and it infers more realistic output for real-life scenarios. To avoid the severe effect of Magnetic Field and Temperature levitation in the eco-system, it has to be predicted by design engineers for establishing the high voltage substation [10–13, 33].

In this paper, load transfer coupled physics mechanism is used for the magnetic, thermal and mechanical effect. The load is transferred between the different physics environment. The unidirectional load transfer method is utilized for M-T-S analysis. The thermal and mechanical analysis is derived from magnetic field analysis. The pictorial representation is shown in figure 1.

The analytical formula for coupled field analysis is established to obtain the relation between temperature rise and structural deformation concerning input current and shape of the material. This formula will provide a direct solution for heterogeneous materials which will be helpful to safeguard the neighbouring equipment in the substation.

The magnetic flux density (B) is calculated from

$$B = \frac{\mu_0 I}{2\pi r} \times \frac{(r^2 - r_i^2)}{(r_o^2 - r_i^2)}. \tag{1}$$

I—Input current to the busbar in A

　r_i—inner radius of the busbar in mm

　r_o—outer radius of the busbar in mm.

　The magnetic force is calculated from

$$F = BIl \sin \theta, \tag{2}$$

where l—length of the conductor.

　The temperature rise is obtained from I^2R loss of the busbar by referring equations (3) and (4).

　For 2D Analysis,

$$I^2Rt = M \times C_P \times \Delta T. \tag{3}$$

For 3D Analysis,

$$I^2Rt = \rho \times C_P \times \Delta T. \tag{4}$$

M—Mass of the busbar in Kg

　ρ—Density of the material kg mm^{-3}

　C_P—Specific heat of the material

　$\Delta T = (T_2 - T_1)$

　T_2—Temperature rise in the busbar in Kelvin

　T_1—Ambient temperature in the busbar in Kelvin.

　The thermal flux and thermal gradient are calculated from following analytical equations (5) and (6).

$$\text{Thermal Flux or Heat Flux} = KA\left(\frac{T_2 - T_1}{d}\right) \tag{5}$$

$$\text{Thermal gradient} = \frac{T_2 - T_1}{dX}, \tag{6}$$

where K = thermal conductivity in W/mm k

　A = area of the surface in mm^2

　d = inner wall thickness in mm

　T_1 = ambient temperature in busbar in Kelvin

　T_2 = Temperature rise in busbar in Kelvin.

　dX = distance measured between the two points of thermal radiation.

　The structural deformation is calculated from thermal stress and strain using equation (7)–(9). The change in length also calculated from strain equation. The mechanical analysis is beneficial in the prediction of structural deformation due to short circuit conditions

$$\text{stress } (f) = E \times \alpha \times \Delta T. \tag{7}$$

From equation (7)

$$\text{strain } (\varepsilon) = \frac{F}{E} = \alpha \times \Delta T, \tag{8}$$

$$\Delta l = \alpha \times \Delta T \times l \tag{9}$$

E—Young's modulus of the material

　α—Coefficient of thermal expansion

　$\Delta l = (l_2 - l_1)$

　F—Force on the area

　l_2—length increment in mm due to thermal stress
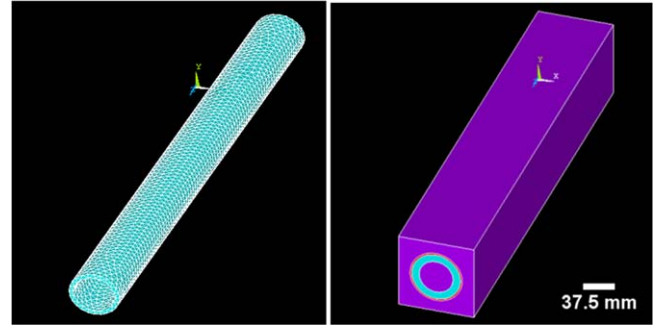
　l_1—Initial length of the busbar in mm.

Figure 2. 230 kV Switchyard busbar model and meshing.
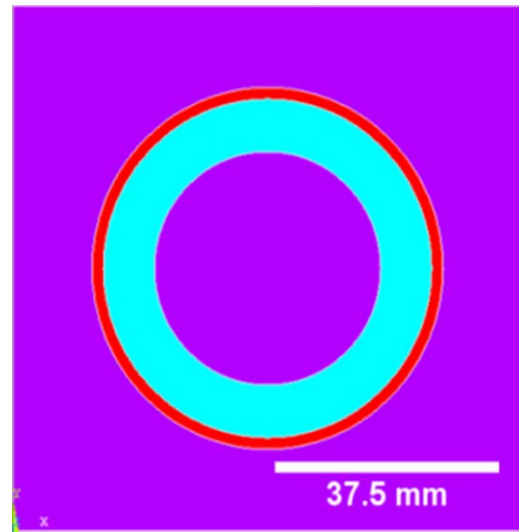

Figure 3. Front view of the busbar with the coating material.

4. Simulation modeling

The 230 kV aluminium busbar has been modelled and meshed in 3D structure by using ANSYS package shown in figure 2. The inner radius and outer radius of the busbar are 37.5 and 45.5 mm. The length of the busbar is 1 m. Numerical methods have come into the frame for more complex problems like different materials. The 6061-T6 Aluminium Alloy has taken for simulation modelling. It has higher mechanical strength and electrical properties.

　In the bare and nano coated busbar, the M-T-S and M-S analysis have been done in the sequential FEM coupling manner. The material selection magnetic, thermal, structural properties and Proper Boundary Conditions (BC) are considered as inputs with air boundary with referring to IEEE std. 738-2012 [32]. The busbar both ends are fixed. In modelling after meshing, the whole model has 68766 elements and the conductor has 27670 elements.

　Figure 3 shows the busbar, coated with nano Fe powder in 0.1 mm thickness. The M-T-S analysis has done for bare and coated busbar in static conditions. The magnetic, Thermal and structural results are compared for bare and nano coated busbars. The outcome simulation results are shown from the average minimum value to the average maximum value.
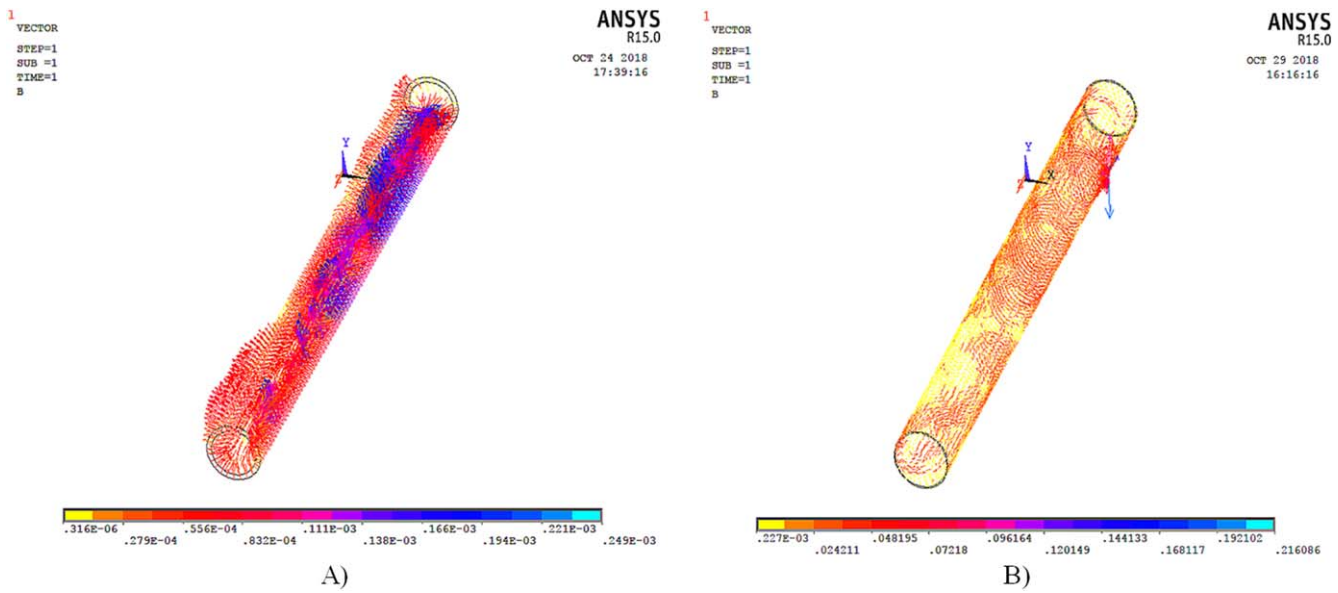
Figure 4. Magnetic flux density (A) bare busbar (B) coated busbar.

Table 1. Material properties.

Properties		Aluminum	Air	Nano Fe
Magnetic properties	Magnetic permeability	1.0022	1	5500
	Resistivity (Ω mm)	2.65×10^{-5}	3.3e + 19	9.7×10^{-6}
Thermal properties	Thermal conductivity (W mm^{-1} K)	0.205	0.24×10^{-4}	0.024
	Specific heat (J Kg^{-1} K^{-1})	900	1004	135
Structural properties	Young's modulus (N mm^{-2})	69000	0.101	13000
	Poisson's ratio	0.32	0.1	0.33

Table 1 shows the physical parameters of the material which are used in the simulation.

4.1. Magnetic analysis

The 1000 A current rating is assigned for input to obtain the results of magnetic field, magnetic flux density and magnetic force. The magnetic field is governed by Maxwell's governing equations (10) and (11)

$$\nabla^2 A = -\mu J, \tag{10}$$

$$\frac{1}{\mu}\left[\frac{\partial}{\partial x}\left(\frac{\partial A}{\partial x}\right) + \frac{\partial}{\partial y}\left(\frac{\partial A}{\partial y}\right) + \frac{\partial}{\partial z}\left(\frac{\partial A}{\partial z}\right)\right] = -J, \tag{11}$$

where, A = magnetic field vector

μ = permeability of material

J = current density.

The results are obtained from the magnetic analysis shows the magnetic field effect in the environment and magnetic force in the busbar displays in figures 4–6. The maximum values of magnetic flux density, magnetic field intensity and magnetic force are 0.35×10^{-6} Wb mm^{-2}, 198 A mm^{-1} and 1.44 N A^{-1} mm in bare conductor shows in figures 4(A), figure 5(A), figure 6(A) respectively. Table 2

shows the permissible value for the magnetic field at power frequency. These values are compared with simulated values.

In the coated busbar, the magnetic field effect has got reduced due to the high permeability and high conductivity material. The composite permeability plays a major role in the magnetic shielding of the busbar. The shielding provides a low resistance path to the magnetic flux lines. Due to high permeability, the magnetic flux density increases more in the coating area than in the atmosphere explain in figure 4(B). The magnetic field intensity is 16 A mm^{-1} shows in figure 5(B). It proves that the magnetic field exposure to the human being is reduced after shielding. It will be beneficial for working persons in the substation for a long time.

The magnetic force is the mechanical force experienced by the current carrying conductor in a magnetic field. In the bare conductor, the high magnetic force is encounter in the surface of the busbar. In figure 6(B), the FEM model shows the minimum magnetic force 0.235×10^{-3} in the surface of the busbar. At the busbar ends, the Lorentz force acting in the longitudinal direction. The magnetic lines of force are passing through the coating material. When the magnetic field strength is reduced in the busbar, the magnetic force on the surface has got reduced. Hence the mechanical stress is
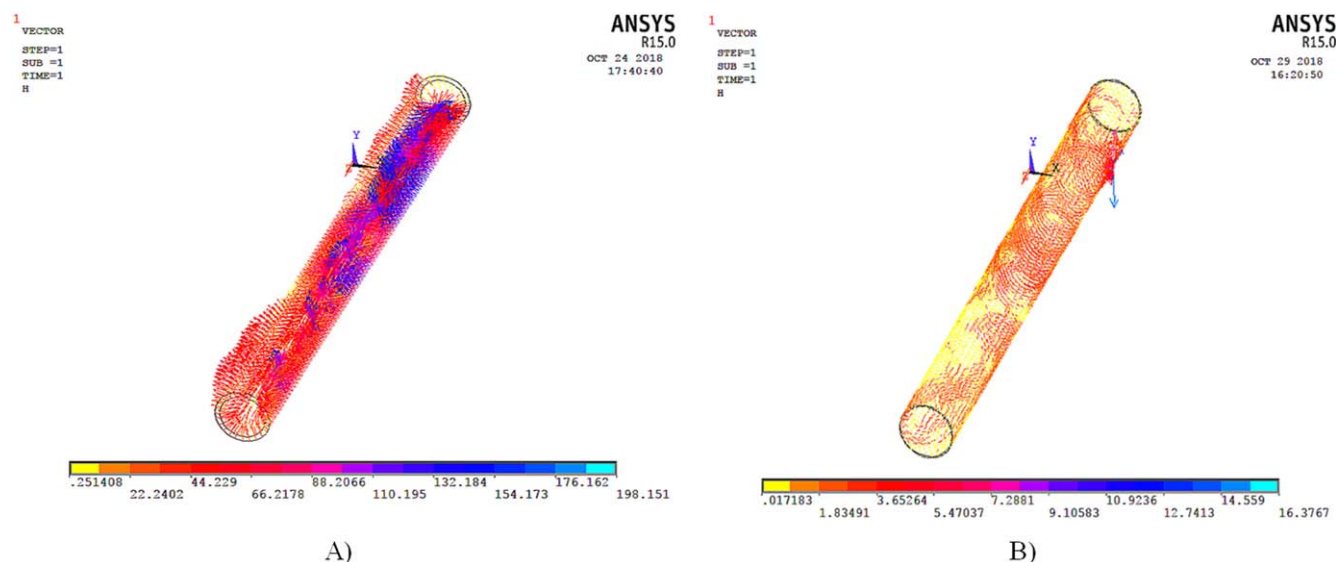
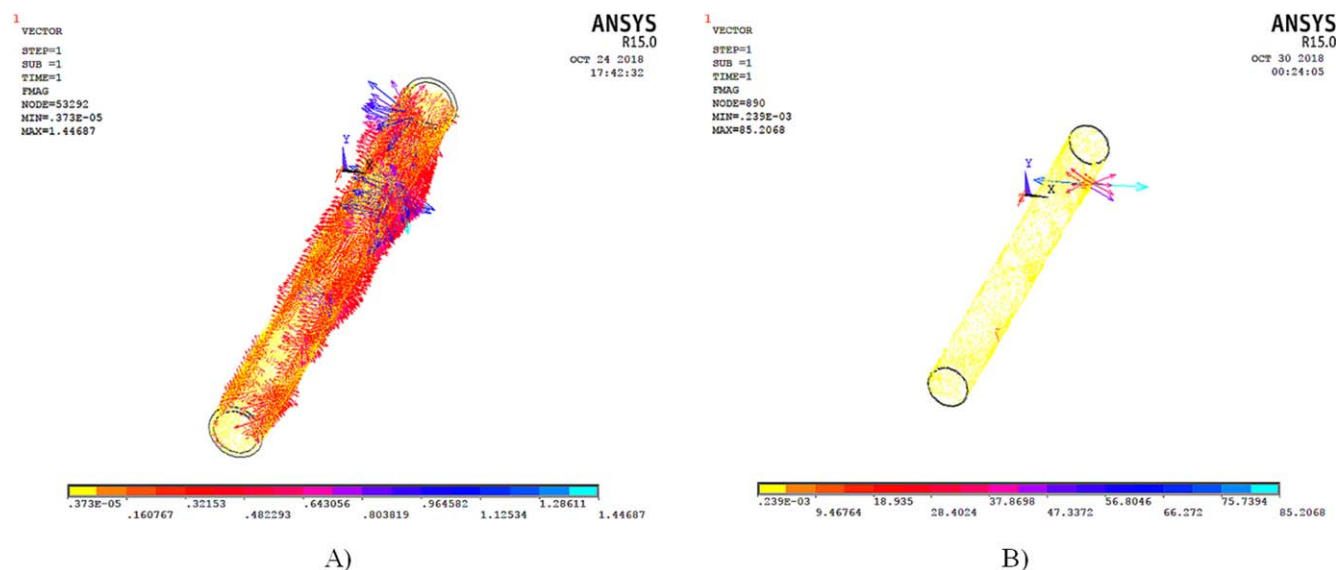**Figure 5.** Magnetic field intensity (A) bare busbar (B) coated busbar.

Figure 6. Magnetic force (A) bare busbar (B) coated busbar.

Table 2. ICNIRP guidelines for magnetic field at power frequency (50 Hz).

	Magnetic field
Public exposure	0.1 mT
Occupational exposure	0.5 mT

reduced in the busbar. The magnetic force is a vital parameter in the short circuit analysis.

4.2. Thermal analysis

In thermal analysis temperature rise, thermal gradient and thermal flux results are obtained through magnetic analysis results. The temperature rise shows the heat loss [29] in the busbar. It is initiated by applying the maximum current. The magneto-thermal is the weak coupling mechanism.

The busbar temperature will not exceed 30 °C from the ambient temperature. The working temperature of the busbar is maintaining below 75 °C. This working temperature of the busbar will not lead to thermal expansion in the aluminium and iron. If current carrying capacity is increased, the cross sectional area of the busbar is increased. So the interface between the aluminium and iron will not lead to thermal stress.

The ohmic losses are calculated from this analysis. It includes heat dissipation and temperature rise of the busbar. Heat dissipation mainly depends on the thermal conductivity of the material. The heat balance equation (12) describes the principle of conservation of energy derived from the first law of thermodynamics.
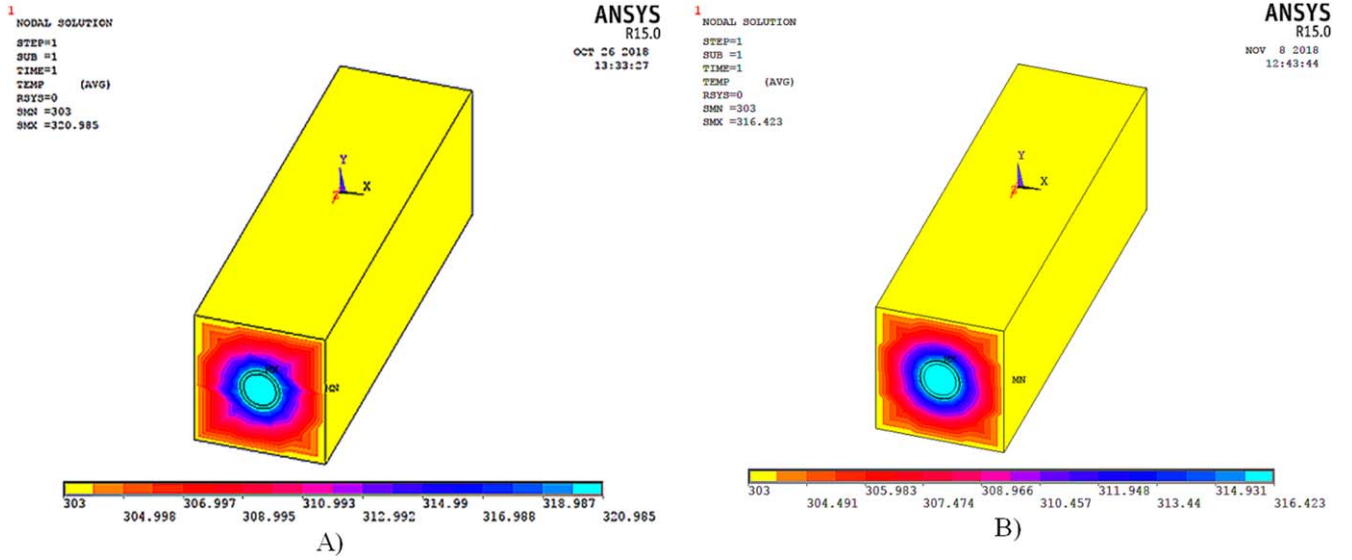
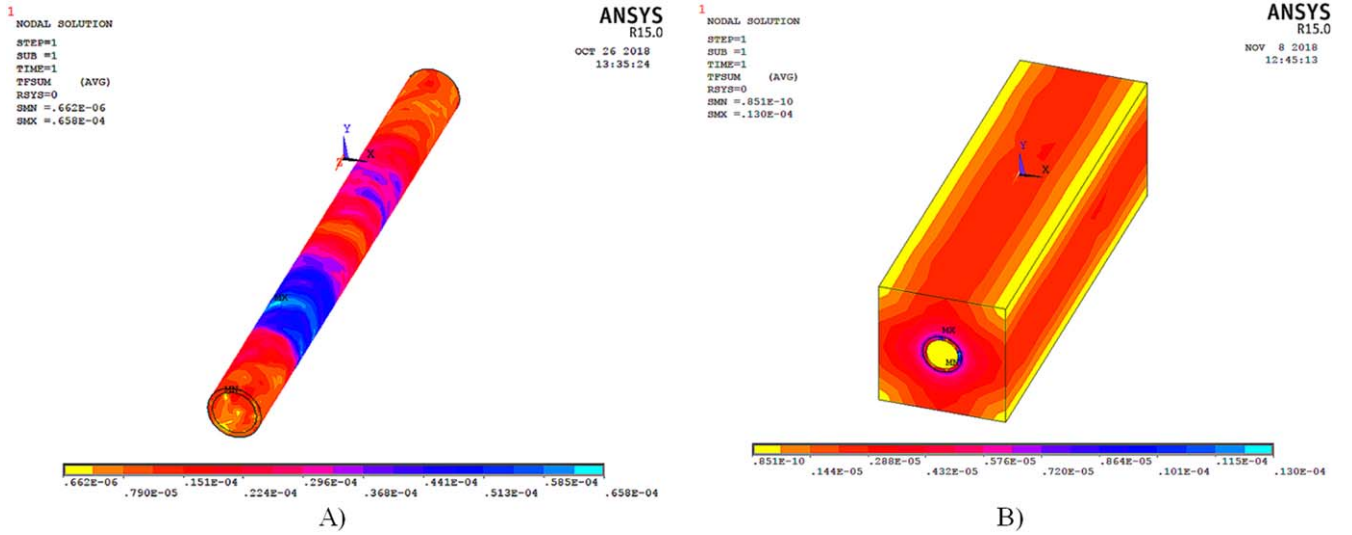**Figure 7.** Temperature rise (A) bare busbar (B) coated busbar.

Figure 8. Thermal flux (A) bare busbar (B) coated busbar.

The thermal governing equation is

$$\left.\begin{array}{l} \partial/\partial x\left[kx\left(\dfrac{\partial T}{\partial x}\right)\right]+ \\[2mm] \partial/\partial y\left[ky\left(\dfrac{\partial T}{\partial y}\right)\right]+ \\[2mm] \partial/\partial z\left[kx\left(\dfrac{\partial T}{\partial z}\right)\right]+Q(x,y,z) \end{array}\right\} = \rho C_p\left(\frac{\partial T}{\partial t}\right), \qquad (12)$$

where q is heat generation, ρ is the density of the material, C_p is the Specific heat of the material and t is the time.

The results exhibit in figures 7(A), 8(A), 9(A) reveal the average values of temperature, thermal flux and thermal gradient as 320.985 K, 0.22×10^{-3} W mm^{-2} and 0.73668 K mm^{-1} respectively of the bare conductor. Due to the high thermal conductivity of the coating material, thermal flux and temperature are decreased after magnetic shielding. It illustrates in

figures 7(B) and 8(B). Figure 9(B) explains the thermal gradient which is related to the heat flux vector using Fourier's law.

The thermal radiation is influenced by electromagnetic waves. The convective and radiative thermal energy directly proportional to the rise in temperature of the busbar. Thermal conductivity of the shielding material influences the Heat dissipation on the outer surface area of the busbar. The intensity of the thermal radiation depends upon the temperature of the emitting surface. Due to the surface temperature reduction, the radiant heat emission from nano coated busbar is considerably reduced as 50 W m^{-2}.

4.3. Structural analysis

Mechanical stress and strain are vital parameters for the electrical equipment in the substation. In steady-state condition, temperature rise leads to mechanical stress. In M-T-S analysis,
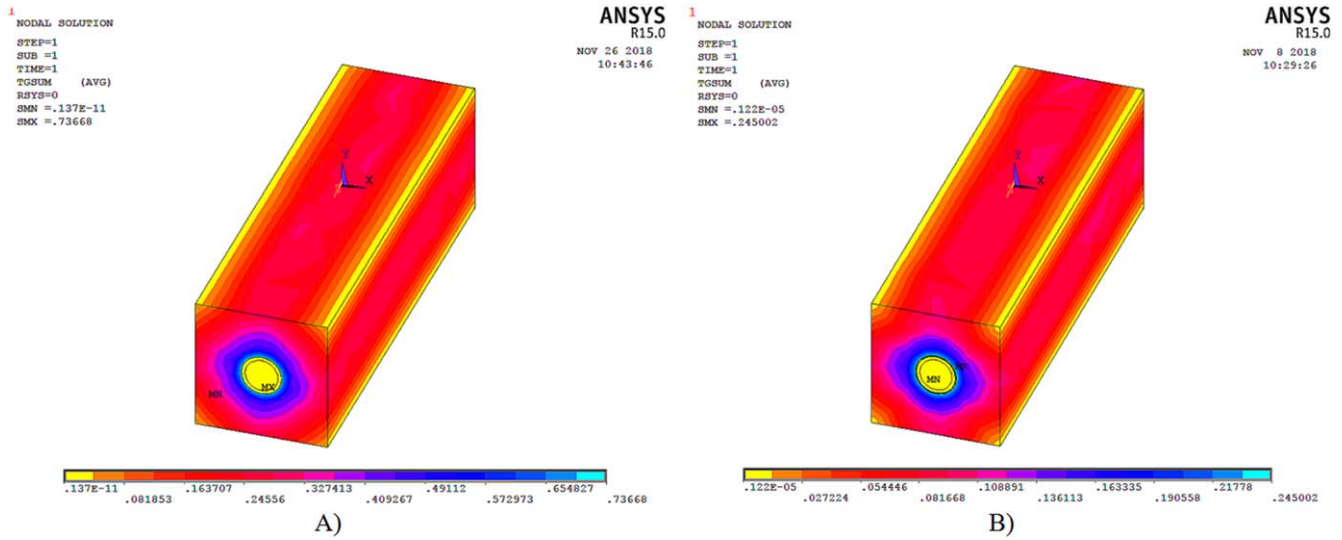
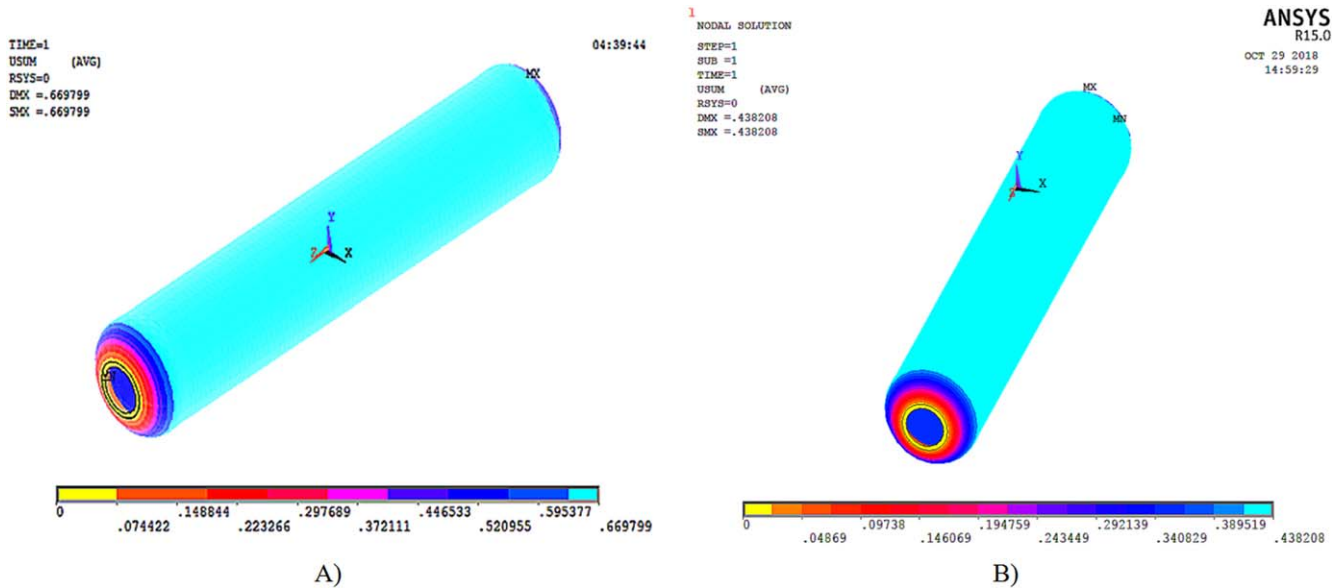**Figure 9.** Thermal gradient (A) bare busbar (B) coated busbar.

Figure 10. Deformation Structure (A) bare busbar (B) coated busbara.

thermal stress is feed as input for structural deformation. The governing equation (13) is used to reveal the displacement structure due to thermal expansion or contractions

$$EA\left(\frac{\partial^2 u}{\partial x^2} + \frac{\partial^2 u}{\partial y^2} + \frac{\partial^2 u}{\partial z^2}\right) = -F, \qquad (13)$$

where

E = young's modulus of the material
A = area of cross section
F = force exerted
u = displacement of structure.

The busbar both ends are fixed. In figure 10(A), demonstrates the mechanical tension due to temperature effect. In the substation, high current is passing throughout the day in electrical equipment. The temperature rise is

directly proportional to thermal radiation and mechanical stress. The mechanical stress is reduced by 35% for the coated busbar which is disclosed in figure 10(B). If the rate of temperature rise (ΔT) is reduced, the busbar will be prevented from deformation. If the busbar is subjected to high mechanical tension continuously, the changes in the right of way (ROW) and degradation are possible. It should be avoided while designing substation. Then the ageing of the busbar is also decreased due to low mechanical stress and thermal stress.

4.4. Magneto-structural analysis

The M-S analysis explains the structural deformation due to magnetic force. In governing equation (13), the force is representing as the magnetic force which is obtained from the
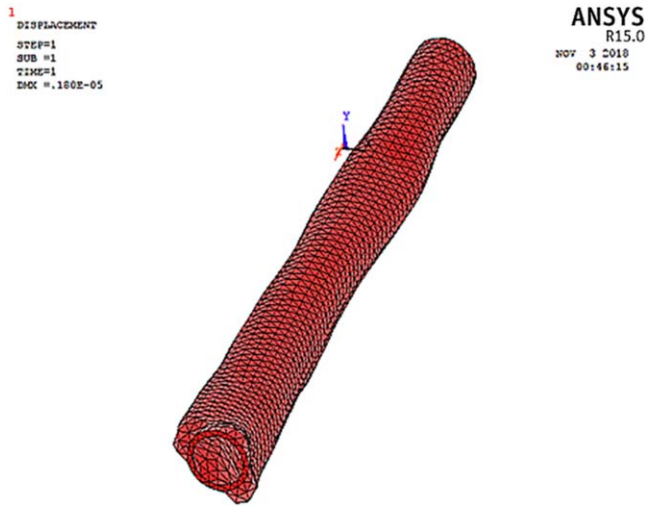
Figure 11. Deformation structure.

Table 3. Comparison of deformation structure due to temperature rise and magnetic force.

Property	Magnetic-thermal-structural	Magnetic-structural
Deformation (mm)	0.669	0.18×10^{-5}

magnetic analysis. The magnetic force is directly provided as input to the structural analysis.

$$\begin{bmatrix} [K] & [0] \\ [0] & [M] \end{bmatrix} \begin{Bmatrix} \{A\} \\ \{u\} \end{Bmatrix} = \begin{Bmatrix} \{J\} \\ \{F_{\text{mech}} + F_{\text{mag}}\} \end{Bmatrix} \quad (14)$$

K, M—Magnetic and mechanical stiffness matrices

    A—Magnetic vector potential from magnetic analysis

    u—Displacement vector potential

    J—Current density

    F_{mech} and F_{mag}—Mechanical force and magnetic force.

In weak coupling, the equation (14) is used for coupled field analysis. For M-S analysis, the F_{mag} is only considered to derive mechanical stress. In table 3 the deformation results are compared with the M-T-S sequential coupling.

Figure 11 explains the mechanical stress due to magnetic force. The value of deformation from the magnetic force is very low in comparison with thermal stress. The stress due to magnetic effect can be eliminated at the steady-state condition. It is concluded that thermal effects are contributing to the maximum deformation. This result derived should be utilized for minimizing the temperature rise at steady-state conditions to reduce the effect of heat flux. But in short circuit condition, the electromagnetic force is high and mechanical stress could worsen by high current. The M-S analysis should be considered at short circuit scenario.

The analytical values are calculated from equations (1)–(9) and compared with simulated values acquired from FEM analysis in table 4 and shown in figure 12. The magnetic, thermal and structural parameter of bare and nano coated busbar are compared. It exhibits a significant reduction in the

magnetic field and thermal radiation in the ecosystem which is hazardous to the human being and global warming. The magnetic and thermal properties of the shielding material take part in the vital role. The shielding material is also economical compared with other soft magnetic alloys. Table 4 shows the less error percentage between the analytical and simulated values. From the integrated formula, the thermal and mechanical strain is calculated for higher current or voltage values.

5. Conclusion

A detailed investigation was carried out to determine the magnetic, thermal and mechanical parameters by using electrical input. This work proposes the magnetic shielding at power frequency. The integrated coupled formula was derived for analytical analysis is compared with the FEM simulation of M-T-S multiphysics analysis. The multiphysics analysis was effectively utilized for both bare and nano iron coated busbar. The obtained simulation results were compared with the analytical values. The outcome of the magnetic, thermal and structural analysis will be helpful for effective design of the high voltage busbar.

From the M-T-S analysis, comparing the coated busbar with the bare busbar, the magnetic field, Thermal flux and mechanical stress were significantly reduced. Due to the high permeability of the shielding material, the magnetic flux density is increased in the coating area. So the Magnetic field pollution is reduced in the environment by 80%. The magnetic field intensity and the magnetic force are also diminished. The magnetic force in the surface of the bare and coated busbar is $0.16\,\text{N A}^{-1}$ mm and $0.23 \times 10^{-3}\,\text{N A}^{-1}$ mm respectively. The magnetic force in the coated busbar is reduced due to low magnetic field strength. It will reduce the magnetic stress in the conductor.

The thermal analysis shows the temperature rise and thermal radiation in the busbar. The rise in temperature against the amount of current is relying on the geometry and material selection of the busbar. In this 230 kV busbar, the temperature rise is reduced by 4 °C in the coated conductor. The thermal radiation is directly proportional to the temperature difference $(T_2 - T_1)$. Subsequently, the temperature reduction leads to low thermal flux. Heat flux in the coated busbar is considerably decreased by $50\,\text{W m}^{-2}$.

From structural analysis, Mechanical stress is obtained for both bare and nano coated busbar. In the shielded busbar, the deformation is reduced by 35%. From M-T-S analysis, the temperature rise is the root cause for the structural deformation at the steady-state condition. The thermal stress followed by structural deformation will enhance the ageing of the electrical equipment. The M-S coupled field analysis shows up at short circuit condition. Electromagnetic elimination from the environment is not possible but shielding achieved the reduction in electromagnetic and thermal stress. This analysis is being extended for NANOPERM (FeNbB) at power frequency magnetic shielding in the substation under steady-state and short circuit conditions.
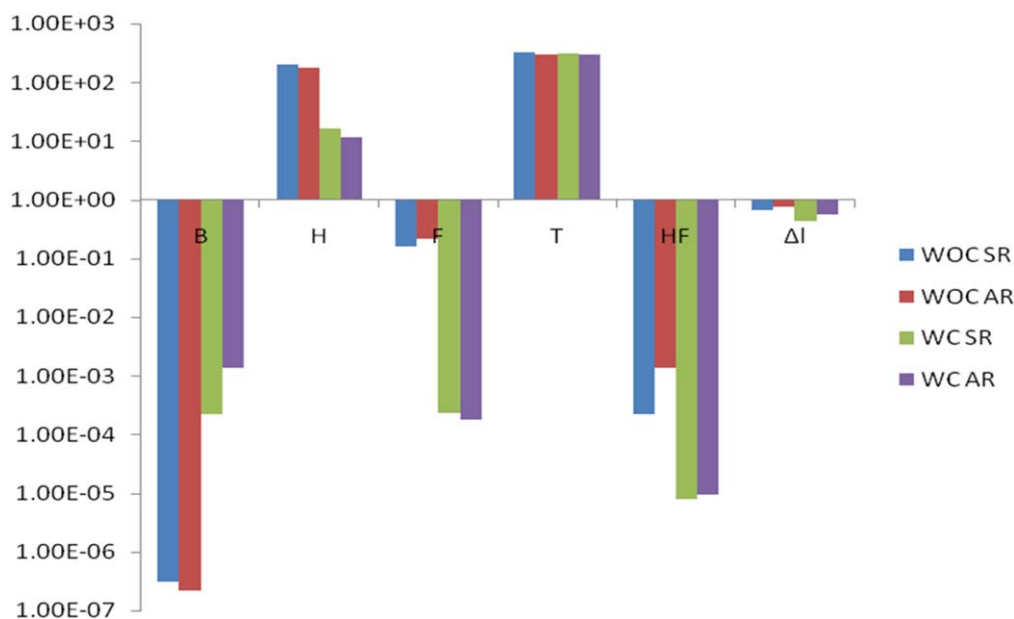
Figure 12. M-T-S analysis comparison between bare and coated conductor.

Table 4. Comparison between simulated and analytical results for bare and nano coated busbar conductor.

Properties	Without coating (WOC)		With coating (WC)	
	Simulated results (SR)	Analytical results (AR)	Simulated results (SR)	Analytical results (AR)
Magnetic flux density (B) (Wb mm^{-2})	0.31×10^{-6}	0.22×10^{-6}	0.22×10^{-3}	1.34×10^{-3}
Magnetic field intensity (H) (A mm^{-1})	198.151	175	16.37	11.45
Magnetic force (MF) (N/A mm)	0.16	0.22	0.23×10^{-3}	0.18×10^{-3}
Temperature (T) (K)	320.985	303.004	316.42	305.008
Thermal flux (HF) (W mm^{-2})	0.22×10^{-3}	1.34×10^{-3}	0.079×10^{-4}	0.0961×10^{-4}
Deformation (Δl) (mm)	0.669	0.75	0.438	0.56

ORCID iDs

S Victoria Mary ⬢ https://orcid.org/0000-0003-0690-3430

References

[1] EPRI Transmission AC Line Reference Book—200 kV and Above Third edition December 2005 R J Lings 1011974

[2] Cheikh M, Vassilieff Y, Fortes A, Benbouhout R and Folign´ H´e 2017 Human body exposure to low frequency wireless charging: direct coupling mechanisms and interferences with medical devices *Progress In Electromagnetics Research Symp.—Fall (PIERS—FALL)* pp 1048–54

[3] (International Commission on Non-Ionizing Radiation Protection) Committee. 1998 Guidelines for limiting exposure to time varying electric, magnetic and electromagnetic fields (up to 300 GHz) *Health Phys.* **74** 494–522

[4] Belmore Park Zone substation EMF study 2008 Magshield Products (Aust.) International Pty. Ltd, EMF report

[5] IEEE Standard for Safety Levels With Respect to Human Exposure to Electromagnetic Field, 0–3 kHz 2002 *IEEE* C95.6

[6] Li N, Yang X and Peng Z 2013 Measurement of electric fields around a 1000 kV UHV substation *IEEE Trans. Power Delivery* **28** 2356–62

[7] Liao J, Peng Z, Li N and Wu H 2015 E-field distribution of circuit with value controlled reactors in 750 kV substations *IEEE 11th Int. Conf. on the Properties and Applications of Dielectric Materials (ICPADM)* pp 572–5

[8] Substation EMC standards, November 2004 EPRI 1008707

[9] Further Discussion and proposed changes 2005 EPRI 1011662

[10] Measuring and Managing Substation EMC Non-Relay equipment 2005 EPRI technical update report 1010744

[11] Measurement of Radio Frequency Interference from High Voltage Substations Backgrounds and Considerations for Future Emission Requirements 2008 CIGRE Position Statement

[12] Li Y *et al* 2018 3D Multi-field coupling analysis of three-phase GIS Bus Bar *IOP Conf. Ser.: Mater. Sci. Eng.* **423** 012136

[13] Kadkhodaei G, Sheshyekani K and Hamzeh M 2016 Coupled electric-magnetic-thermal-mechanical modelling of busbars under short-circuit conditions *IET Gener. Transm. Distrib.* **10** 955–63

[14] Kadkhodaei G, Sheshyekani K, Hamzeh M and Tavakoli S 2016 Multiphysics analysis of busbars with various arrangements under short-circuit condition *IET Electr. Syst. Transp.* **6** 237–45

[15] Smirnova L, Juntunen R, Murashko K, Musikka T and Pyrhonen J 2016 Thermal analysis of the laminated busbar

system of a multilevel converter *IEEE Trans. Power Electron.* **31** 1479–88

[16] Victoria Mary S and Pugazhendhi Sugumaran C 2018 Diagnosis on magnetic-thermal field emission of 440 kV busbar with nano coating *IEEE-INAE Workshop on Electromagnetics-IIWE*

[17] Sawa T and Nakagawa K 1994 Soft magnetic properties of ultra thin Fe-based amorphous alloy cores *Mater. Sci. Eng.* **181–182** 902–5

[18] Bavastro D, Canova A, Giaccone L and Manca M 2014 Numerical and experimental development of multilayer magnetic shields *Elsevier Electr. Power Syst. Res.* **116** 374–80

[19] Giselher H 2013 Modern soft magnets: amorphous and nanocrystalline materials *Elsevier Acta Mater.* **61** 718–34

[20] Chrobak A, Kaleta A, Kwapuliński P, Kubisztal M and Haneczok G 2012 Magnetic shielding effectiveness of iron-based amorphous alloys and nanocrystalline composites *IEEE Trans. Magn.* **48** 1512–5

[21] Zhao W N, Yang X J, Yao C, Ma D G and Tang H J 2007 Magnetic shielding design for coupler of wireless electric vehicle charging using finite element analysis *IOP Conf. Series: Earth Environ. Sci.* **86** 012039

[22] Gozzelino L, Agostino A, Gerbaldo R, Ghigo G and Laviano F 2012 Magnetic shielding efficiency of superconducting/ferromagnetic systems *IOP Publ. Supercond. Sci. Technol.* **25** 115013

[23] Kvitkovic J, Pamidi S and Voccio J 2009 Shielding AC magnetic fields using commercial YBa$_2$Cu$_3$O$_7$-coated conductor tapes *IOP Publ. Supercond. Sci. Technol.* **22** 125009

[24] Xia D and Xia Z 2015 Performance analysis of superconducting generator electromagnetic shielding *IOP Conf. Ser.: Mater. Sci. Eng.* **101** 012027

[25] Kuznetsov B, Bovdui I and Nikitina T 2019 System of active shielding of magnetic field of power transmission lines with different spatial location of shielding coil *IEEE 2nd Ukraine Conf. on Electrical and Computer Engineering* pp 275–8

[26] Kim S W, Kim H H, Hahn S C, Lee B Y, Park K Y, Shin Y J, Song W P, Kim J B and Shin I H 2002 Coupled finite-element–analytic technique for prediction of temperature rise in power apparatus *IEEE Trans. Magn.* **38** 921–4

[27] Yamazaki K and Aoki A 2016 3D electromagnetic field analysis combined with mechanical stress analysis for interior permanent magnet synchronous motors *IEEE Trans. Magn.* **52** 3

[28] Zhiming H, Yifan Z, Yi J, Mingli F, Guoli W, Ran Z and Qiao W 2019 Study on the influence of harmonics on the magnetic leakage field and temperature field of 500 kv connected transformer *2nd Int. Conf. on Electrical Materials and Power Equipment—Guangzhou—China* pp 596–600

[29] Kyoung Kim J, Chin Hahn S, Yop Park K, Kyu Kim H and Ho Y 2005 Temperature rise prediction of EHV GIS bus bar by coupled magnetothermal finite element method *IEEE Trans. Magn.* **41** 1636–9

[30] Ahn H-M, Oh Y-H, Kim J-K, Song J-S and Hahn S-C 2012 Experimental verification and finite element analysis of short-circuit electromagnetic force for dry-type transformer *IEEE Trans. Magn.* **48** 819–22

[31] Prakash Alapati S S and Kulkarni S V 2009 Coupled magnetic-structural finite element analysis *Excerpt from the Proc. COMSOL Conf.*

[32] IEEE Standard for Calculating the Current-Temperature Relationship of Bare Overhead Conductors, IEEE Power and Energy Society, IEEE Std. 738-2012

[33] Kumbhar G B and Mahajan S M 2009 Field-circuit coupled formulation of transient phenomena in current transformers *IEEE Power & Energy Society General Meeting* (Calgary, Alberta, Canada)